INVESTIGATING SHOCK DEFORMATION IN A SUITE OF LAUNCH-PAIRED MARTIAN SHERGOTTITES.

R. R. Patel[1], G. Benedix[1,2], and L. Forman[1], [1]Space Science & Technology Centre, School of Earth and Planetary Sciences, Faculty of Science and Engineering, Curtin University, Bentley, Western Australia, 6102 (ravi.patel@postgrad.curtin.edu.au), [2]Planetary Science Institute, 1700 East Fort Lowell, Tucson, AZ 85719-2395, USA.

Introduction: The study of martian meteorites has significantly impacted the planetary science community over recent decades and has helped to build a greater understanding of the surface geology and impact processing on Mars [1]. Currently, there are ~60,000 known meteorites on Earth, with only ~200 known to have originated on Mars. Shergottites make up ~80% of the current terrestrial inventory of martian meteorites. They are mafic to ultramafic igneous rocks with basaltic to lherzolitic compositions [2]. Shergottites are the youngest of all martian meteorites and most likely formed in surficial and/or shallow sub-surface lava flows, potentially within three young volcanic regions on the surface of Mars [2,3,4]. These meteorites are moderately to highly shocked, with substantially higher shock levels than most other meteorites [2]. Shock manifests itself in the deformation of minerals within these meteorites. We have examined 4 shergottites that share the same cosmic ray exposure age (~3.1 Ma) and span different shergottite classes to investigate relative shock deformation of meteorites that likely sample the same location on Mars [2,5,6].

Sample and Methods: Eight thin and thick-sections (either mounted onto 1-inch round thin-section glass slides or embedded in 1-inch round epoxy mounts) of four shergottites were analysed using scanning electron microscopy (SEM) with electron backscatter diffraction (EBSD) techniques, and optical microscopy techniques. The sections analysed were as follows: RBT 04262,24; ALHA 77005,147; Los Angeles, P10075; Los Angeles,746; Los Angeles,750; LAR 06319,32; LAR 12011,27; and LAR 12011,10. Roberts Massif (RBT) 04262 (and its pair RBT 04261) are classified as REE-enriched, permafic, poikilitic shergottites [7]. Allan Hills, Antarctica (ALHA) 77005 is classified as an REE-intermediate, ultramafic, poikilitic shergottite [2]. Los Angeles is classified as an REE-enriched, mafic, diabasic shergottite [2,8]. Larkman Nunataks (LAR) 06319/12011 are paired meteorites and are classified as REE-enriched, permafic, olivine-phyric shergottites [9]. SEM and EBSD techniques were conducted on the TESCAN Mira3 FE-SEM located within the John De Laeter Centre, Curtin University. Optical microscopy was conducted using a Zeiss Axio Imager.M2m Imaging System and a Nikon LV100 Optical Polarising Imaging System, both located in the school of Earth and Planetary Sciences, Curtin University. EBSD data was obtained, processed and reduced using Oxford Instruments software: AZtec and Channel5. EBSD analyses were conducted on a number of regions (including large area maps and high resolution close-up maps), focusing on low- and high-pressure polymorphs of olivine (forsterite with minor fayalite and wadsleyite), pyroxene (pigeonite and augite with minor enstatite and diopside), and opaque phases (ilmenite, chromite, pyrrhotite, pentlandite and titanomagnetite). Phase maps (Fig. 1), grain reference orientation deviation (GROD) angle maps, maximum orientation spread (MOS) maps (Fig. 2), and grain orientation spread (GOS) maps were constructed using Channel5. Recent advances in EBSD data reduction allow for visualization of deformation within crystals by focusing on GROD angles (the angle of deviation, from the average crystallographic orientation of all the pixels within a grain, is determined for each pixel within that grain, for all grains within the mapped area), MOS (the maximum GROD angle of all the pixels within a given grain, for all grains within the mapped area), and GOS (the average of all GROD angles within a given grain, for all grains within the mapped area) [10,11]. GROD, MOS and GOS represent deviations in the crystallographic orientation of crystals (i.e. bending within crystals). The higher the MOS and GOS angle within a crystal, the higher amounts of deformation present. By studying these features, we can contribute to the quantification of the amount of shock deformation present within meteorites.

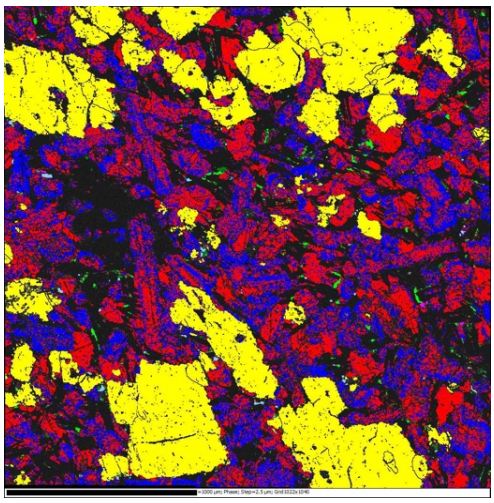

Figure 1: Large area EBSD phase map of LAR 12011,27. Yellow = Forsterite. Red = Pigeonite. Blue = Augite. Black = Maskelynite.

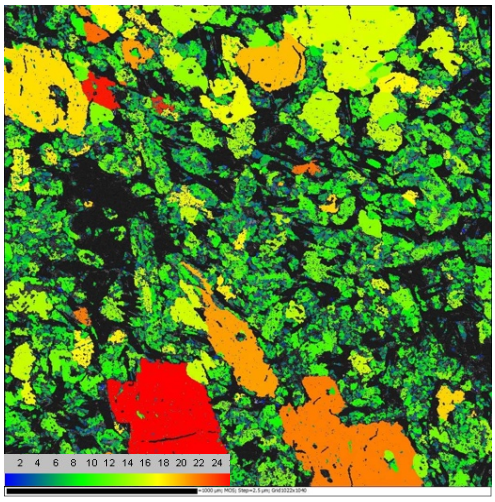

Figure 2: Large area EBSD MOS map of LAR 12011,27. Scaled to a maximum of 26°.

Results and Discussion: We investigated deformation features within plagioclase feldspar, olivine and pyroxene. The majority of the shock deformation features of interest are observed in transmitted light optical microscopy and thus require the use of thin-sections rather than thick-sections. ALHA 77005,147 and LAR 12011,10 are thick-sections, and consequently, certain diagnostic features observed in transmitted light could not be analysed. Therefore, comparing deformation features observed in optical microscopy was not suitable for the comparison of relative deformation. However, a pressure range that the shergottites have been exposed to during the impact event was determined. Plagioclase feldspar is present within all sections and has been melted and recrystallised to form maskelynite, a shock-induced diaplectic glass (which occurs at shock pressures between of 24 to 45 GPa) [11]. No original plagioclase feldspars can be identified within the sections and no observations were made to indicate that the maskelynite has completely melted into 'normal glass'. Since no original plagioclase feldspar is preserved within any of the samples, these shergottites must have experienced shock pressures of at least 24 GPa and above. Planar deformation features (PDF) in olivine are present within RBT 04262, ALHA 77005 and LAR 06319/12011 and form at shock pressures between 30 to 60 GPa [11]. Olivine possesses mosaicism within RBT 04262 and LAR 06319/12011 which occurs at shock pressures between 15 to 65 GPa [11]. Mechanical twinning of pyroxene is present within all the samples and occurs at shock pressures between 5 and 70 GPa [11]. Mosaicism is also present in pyroxene within RBT 04262, Los Angeles and LAR 06319/12011 and occurs at shock pressures between 20 to 70 GPa [11]. Lastly, PDF's are also present in pyroxene within Los Angeles and occurs at shock pressures between 30 to 70 GPa [11]. Therefore, these shergottites must have been exposed to shock pressures, during the launch event, of at least 24 GPa and no more than 70 GPa.

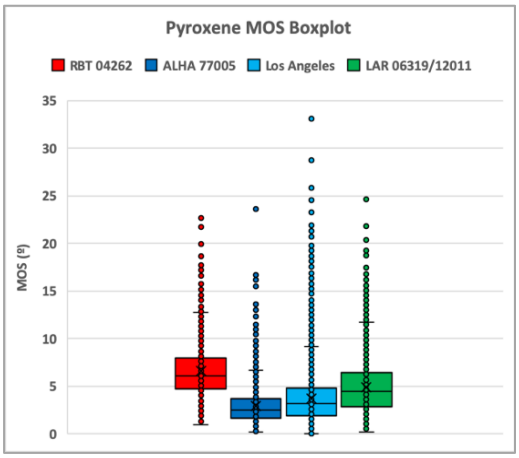

Figure 3: Box and whisker plot representing the MOS distribution in pyroxene within each shergottite.

We determined from the EBSD results that MOS measurements of pyroxene resemble the overall bulk deformation within all the sections, and since pyroxene is present throughout all sections (at similar modal abundances), it is most suitable for the comparison of relative deformation within the shergottites examined in this study (Fig. 3). The maximum pyroxene MOS values are considered outliers and do not represent overall deformation. Therefore, we focused on the average of all pyroxene MOS values as this is most suitable for the comparison of relative deformation. The average of all pyroxene MOS values are; RBT 04262 = 6.61°; LAR 06319/12011 = 4.91°; Los Angeles = 3.76°; and ALHA 77005 = 2.95°. Thus, RBT 04262 demonstrates the highest amount of deviation in the crystallographic orientation of the grains overall (i.e. deformation/bending) and may therefore have been situated closest to the impact site, followed by LAR 06319/12011, Los Angeles, then ALHA 77005 respectively. These findings are preliminary; additional optical microscopy and EBSD analyses is recommended on a larger sample size of thin-sections, focusing on high-resolution close-up maps of pyroxene and trace phases (zircons, reidite, rutile and xenotime) within the samples.

References: [1] Collinet, M. et al. (2017) *GCA*, 207, 277-297. [2] Nyquist, L. E. et al. (2001) *SSR*, 96(1), 105-164. [3] Kiefer, W. S. (2003) *MAPS*, 39, 1815-1832. [4] Tornabene, L. L. et al. (2006) *JOGRP*, 111(E10). [5] Nishiizumi, K. and Caffee, M. (2010) *LPSC XLI*, 2276. [6] Nagao, K. (2008) *METSOC LXXI*, 5200. [7] Usui, T. et al. (2010) *GCA*, 74(24), 7283-7306. [8] Mikouchi, T. (2001) *AMR*, 14, 1-20. [9] Sarbadhikari, A. B. et al. (2009) *GCA*, 73(7), 2190-2214. [10] Ruzicka, A. M. and Hugo, R. C. (2018) *GCA*, 234, 115-147. [11] Stöffler, D. et al. (2018) *MAPS*, 53(1), 5-49.